CCFE-PR(17)47

S. Breton, F.J. Casson, C. Bourdelle, C. Angioni, E. Belli, Y. Camenen, J. Citrin, X. Garbet, Y. Sarazin, and the JET contributors

High Z neoclassical transport : generalized analytical formula for tractable predictive simulations for integrated modeling

High Z neoclassical transport : generalized analytical formula for tractable predictive simulations for integrated modeling

S. Breton[1], F.J. Casson[2], C. Bourdelle[1], C. Angioni[3], E. Belli[4], Y. Camenen[5], J. Citrin[6], X. Garbet[1], Y. Sarazin[1], and JET contributors

[1]CEA, IRFM, F-13108 Saint-Paul-lez-Durance, France.
[2]CCFE, Culham Science Centre, Abingdon, Oxon, OX14 3DB, UK
[3]Max-Planck-Institut für Plasmaphysik, Garching, Germany
[4]General Atomics, PO Box 85608, San Diego, CA 92186-5608, USA
[5]Aix-Marseille Université, CNRS, PIIM UMR 7345, 13397 Marseille Cedex 20, France and
[6]FOM Institute DIFFER: Dutch Institute for Fundamental Energy Research, PO Box 6336, 5600 HH Eindhoven, The Netherlands

High Z neoclassical transport : generalized analytical formula for tractable predictive simulations for integrated modeling

S. Breton[1], F.J. Casson[2], C. Bourdelle[1], C. Angioni[3], E. Belli[4], Y. Camenen[5], J. Citrin[6], X. Garbet[1], Y. Sarazin[1], the JET contributors*

EUROfusion Consortium, JET, Culham Science Centre, Abingdon, OX14 3DB, UK

[1]*CEA, IRFM, F-13108 Saint-Paul-lez-Durance, France.*

[2]*CCFE, Culham Science Centre, Abingdon, Oxon, OX14 3DB, UK*

[3]*Max-Planck-Institut für Plasmaphysik, Garching, Germany*

[4]*General Atomics, PO Box 85608, San Diego, CA 92186-5608, USA*

[5]*Aix-Marseille Université, CNRS, PIIM UMR 7345, 13397 Marseille Cedex 20, France and*

[6]*FOM Institute DIFFER: Dutch Institute for Fundamental Energy Research, PO Box 6336, 5600 HH Eindhoven, The Netherlands*

(*See the author list of "Overview of the JET results in support to ITER" by X. Litaudon et al. to be published in Nuclear Fusion Special issue: overview and summary reports from the 26th Fusion Energy Conference (Kyoto, Japan, 17–22 October 2016))

Heavy impurities, such as tungsten (W), can exhibit strongly poloidally asymmetric density profiles in rotating or radio frequency heated plasmas. In the metallic environment of JET, the poloidal asymmetry of tungsten enhances its neoclassical transport up to an order of magnitude, so that neoclassical convection is expected to dominate over turbulent transport. The modeling of poloidal asymmetries is hence necessary in the integrated modeling framework. The neoclassical drift kinetic code, NEO [E. Belli and J. Candy, Plasma Phys. Control. Fusion P50, 095010 (2008)], takes into account the impact of poloidal asymmetries on W transport. However, the computational cost required to run NEO slows down significatively integrated modeling. An analytical formulation was proposed to describe heavy impurity neoclassical transport in the presence of poloidal asymmetries in specific collisional regimes [C. Angioni and P. Helander, Plasma Phys. Control. Fusion 56, 124001 (2014)]. The present work compares the analytical formula to the numerical results produced with NEO. It investigates if the formula can be used to accurately predict heavy impurity transport in experiment when combined with a neoclassical model that is less CPU intensive but does not include the effect of poloidal asymetries, such as NCLASS [W. A. Houlberg, K. C. Shaing, S. P. Hirshman and M. C. Zarnstorff, Phys. Plasmas 4, 3230 (1997)]. The analytical formulation was derived in the limit where the main ions are in the banana regime, with high-Z trace impurities in the Pfirsch-Schlüter regime. The formula is found to remain valid outside its definition domain. Indeed, considering main ions in the banana regime, it well reproduces NEO results whatever the collisionality regime of impurities, provided the poloidal asymmetry is not too large. However, for very strong poloidal asymmetries, agreement is only obtained for impurities in the Pfirsch-Schlüter regime. Within the integrated transport platform JETTO, it is demonstrated that NEO and the neoclassical formula combined with NCLASS lead to the same tungsten profile predictions while gaining a factor 1100 of CPU time.

I. INTRODUCTION

Tungsten (W) was chosen as a Plasma Facing Component because of its high melting point, its low erosion rate and low hydrogen retention. But due to its large charge number 74, W ions are not fully stripped even in the hot tokamak core, leading to a relatively high degree of line radiation. This means that accumulation of W in the plasma core can be highly deleterious. Above a certain threshold, this leads to the loss of confinement and eventually disruptions. To avoid central W accumulation, an accurate understanding of W transport is a key issue. W transport is both turbulent and neoclassical. In the central region of JET core, W transport has been shown to be mostly neoclassical [1–5], whereas in the outer part the turbulent transport dominates. Due to its large mass A=184, W is subject to a strong centrifugal force when the plasma rotates. This causes poloidal asymmetry in W density. In presence of NBI momentum input, those asymmetries are shown to increase neoclassical W transport by an order of magnitude in JET [5, 6]. Ion Cyclotron Resonance Heating (IRCH) with anisotropic temperature distribution and Radio Frequency heating also impact the poloidal distribution of W up to a factor of 2 [7, 8]. The neoclassical drift kinetic code NEO[9, 10] includes comprehensive treatments of poloidal asymmetries. However the computational cost of running NEO becomes problematic when embedded in integrated modeling platforms such as JETTO [11].

The goal of this work is to study an alternative solution applying an analytical formula that describes the impact of poloidal asymmetries on heavy impurity transport. This formula, combined with the neoclassical code NCLASS [12] in which poloidal asymmetries are not included, offers a faster option in integrated modeling. Based on previous works such as[13, 14] and especially [15], Angioni and Helander proposed such a formula in [16]. It describes the impurity neoclassical flux with a simplified collision model, for main ion in banana regime, impurity in trace limit and collisional Pfirsch-Schlüter regime and low main ion Mach number. These constraints are not all simultaneously fulfilled in experimental plasmas. It is therefore essential to explore the validity domain of the analytical formulation up to realistic ranges. JET-ILW plasmas are used as an illustration of such realistic conditions. This formula was tested out of its validity domain against NEO for several parameter scans, in order to test its robustness and its limits, and it is found to remain valid outside its definition domain. Indeed, considering main ions in the banana regime, it well reproduces NEO results whatever the collisionality regime of impurities, provided the poloidal asymmetry is not too large. However, for very strong poloidal asymmetries, agreement is only obtained for impurities in the Pfirsch-Schlüter regime.The final test is to use the formula, combined with NCLASS inside the transport solver JETTO to simulate a discharge, and then compare the result with an integrated simulation with NEO, while gaining about a factor 1100 of CPU time.

The analytical formula and its limits are introduced in Section 2 and is generalized. In section 3 the formula is tested against NEO for one JET pulse. A reconstruction of W transport coefficients is made using analytical terms. The goal is to explore how the formula behaves compared with the code, to see and understand its limits. Finally in section IV the formula is tested inside JETTO and compared with a run carried out using NEO.

II. NEOCLASSICAL FORMULA

This section focuses on the theoretical expression for the neoclassical impurity flux in presence of poloidal asymmetries. The theoretical formula is introduced and the limits in which it is derived are discussed.

A. Neoclassical flux of heavy impurities with poloidally asymmetric density distribution

Neoclassical impurity theory has been generalized to consider the case of poloidally asymmetric heavy impurity such as W [14–20]. The theory is valid whether the W localization is caused by centrifugal forces or RF induced temperature anisotropy. If the trace impurity is in the Pfirsch-Schlüter regime and the main ion is in the banana regime, with a simplified collision operator valid at large aspect ratio, the neoclassical impurity transport can be written as follows (equation (2) of [20], recalled from [16]) :

$$\frac{R\langle\Gamma_Z^{neo}\rangle}{\langle n_Z\rangle} = q^2 D_c Z\left[\left(\frac{1}{Z}\frac{R}{L_{nZ}} - \frac{R}{L_{ni}} + \frac{1}{2}\frac{R}{L_{Ti}}\right)P_A^{model} - 0.33 P_B^{model} f_c \frac{R}{L_{Ti}}\right] \tag{1}$$

with

$$P_A^{model} = \frac{1}{2\varepsilon^2}\frac{\langle B^2\rangle}{\langle n_Z\rangle}\left[\left\langle\frac{n_Z}{B^2}\right\rangle - \left\langle\frac{B^2}{n_Z}\right\rangle^{-1}\right] \tag{2}$$

$$P_B^{model} = \frac{1}{2\varepsilon^2}\frac{\langle B^2\rangle}{\langle n_Z\rangle}\left[\frac{\langle n_Z\rangle}{\langle B^2\rangle} - \left\langle \frac{B^2}{n_Z}\right\rangle^{-1}\right] \tag{3}$$

Γ_Z^{neo} is the neoclassical flux of the impurity charge number Z. R is the major radius, q the safety factor, B the magnetic field, $\varepsilon = {}^r/_R$, r is the minor radius. The gradient length is defined as $\frac{1}{L_X} = -\frac{\nabla_r\langle X\rangle}{\langle X\rangle}$.The label i stands for the main ion, Z for the impurity. With f_c the fraction of circulating particles, $<.>$ means that the quantity is flux surface averaged, and $D_c = \frac{\rho_i^2}{\tau_{ii}}$the diffusion coefficient, valid for the impurity in Pfirsch-Schlüter regime. $\boldsymbol{\rho}^2{}_i = \frac{v_{thi}^2}{\langle\Omega_i^2\rangle}$is the squared larmor radius, $\tau_{ii} = \nu_{ii}^{-1} = 3(2\pi)^{3/2}\frac{\varepsilon_0{}^2 m_i^{1/2} T_i^{3/2}}{n_i e^4 ln\Lambda}$is the main ion-main ion collision time, and the thermal velocity is defined as $v_{th,i} = \sqrt{2T_i/m_i}$.

The structure of equation (1) is very similar to the impurity transport flux without rotation shown in equation (4) (see [21]). When comparing equations (1) and (4), one can recognize the diffusive term proportional to ∇n_Z, the neoclassical pinch driven by ∇n_i, both multiplied by the P_A^{model} factor. Concerning the temperature screening driven by ∇T_i, two terms are contributing : the term without asymmetries multiplied by P_A^{model} to which a new term is added, proportional to P_B^{model}. This new P_B^{model} term decreases the impact of temperature screening. The P_A^{model} and P_B^{model} factors are both purely geometrical and one can notice that without poloidal asymmetries of the impurity density n_Z, i.e. $\langle n_Z\rangle = n_Z$, $P_A^{model} = 1$ and $P_B^{model} = 0$ and one recovers W flux from equation (4) and [21]. In the case of strong asymmetries, P_A^{model} and P_B^{model} increase ; it means that the impurity transport will be more sensitive to the main ion density gradient, and the benefits from temperature screening will be reduced.

B. Theoretical limits and implications

1. *Symmetric neoclassical temperature screening and pinch coefficients*

In [20], the formula for impurity transport is derived with the main ion in the banana regime, and heavy impurities in the Pfirsch-Schlüter regime. Heavy impurities must be present as a trace, i.e. $\alpha = \frac{Z_Z^2 n_Z}{Z_i^2 n_i} \ll 1$. The plasma can rotate, but the main ion Mach number is assumed to be small, ie $M_i \ll 1$ and heavy impurity Mach number $M_Z = O(1)$.

In experimental plasmas, the main ions in banana and impurities in Pfirsch-Schlüter conditions are hardly simultaneously fulfilled (see figure 3 for example based on a JET-ILW pulse). This impacts the numerical value 1/2 in front of $\frac{R}{L_{Ti}}$ inside equation (1), which is valid only in certain collisionality regimes according to [21]. Therefore this value has to be tested before starting the comparison between the formula and NEO.

In Wenzel-Sigmar neoclassical formulation [21], neoclassical impurity flux without rotation, Γ_Z^{PS} with impurity in Pfirsch-Schlüter, is described as follows :

$$\frac{R\Gamma_Z^{PS}}{n_Z} = q^2 D_c Z\left[K\left(\frac{1}{Z}\frac{R}{L_{nZ}} - \frac{R}{L_{ni}}\right) - H\frac{R}{L_{Ti}}\right] \tag{4}$$

$$K = 1 - \frac{0.52\alpha}{0.59 + \alpha + 1.34g^{-2}} \tag{5}$$

$$H = -0.5 + \frac{0.29 + 0.68\alpha}{0.59 + \alpha + 1.34g^{-2}} \tag{6}$$

$$\text{With } \alpha = \frac{n_Z Z_Z^2}{n_i Z_i^2} \text{ and } g = \nu_D^* \epsilon^{3/2},\ \nu_D^* = \frac{\nu_{DD} qR}{v_{th,D}\epsilon^{3/2}}$$

Two coefficients apply, H and K, respectively on the ion density gradient and the main ion temperature gradient. These coefficients depend on the impurity concentration and charge, as well as the main ion collisionality. Equation (1), from [20] assumes that K=1 and H=-0.5, which is true for trace impurity in Pfirsch-Schlüter regime and main ion in banana regime. But as seen later in figure 3, Deuterium is typically in the plateau regime near the magnetic axis and the Last Closed Flux Surface while W is in plateau regime across most of the plasma, except at the edge where it is in Pfirsch-Schlüter regime.

To check if it is adequate to keep K=1 and H=-0.5 in the formula, a scan of the main ion (assumed to be Deuterium) collisionality was made with NEO. The Deuterium density is varied over a large range, in order to vary D collisionality. The ratio ${}^{n_Z}/_{n_D=10^{-6}}$ was kept fixed to maintain the impurity in the trace limit $\frac{n_Z Z^2}{n_D} = 1,2.10^{-3}$ with Z=34 the charge of W. Therefore, the W collisionality is varied from plateau to Pfirsch-Schlüter regimes. Figure 1 shows the ratio H/K versus Deuterium collisionality ν_D^*, as it is not possible with NEO to isolate H and K from the diffusion coefficient D_c. Indeed the theoretical formulation of D_c is only valid for deep Pfirsch-Schlüter regime, which makes it not reliable for a collisionality scan. NEO is also compared with NCLASS ([12]), a neoclassical code based on the fluid moment approach with a simplified collision operator. NCLASS does not take into account poloidal asymmetries. NCLASS uses the Hirschman-Sigmar collision operator , based on pitch angle scattering. NEO ([9, 19, 22]) solves the full drift kinetic equation. It provides a first-principle calculation of the transport coefficients directly from the kinetic solution of the distribution function. It uses the full linearized Fokker Planck collision operator, which is more accurate, especially for multi-species collisions. NEO is also reliable in general geometry. Two NEO scans were made, one with adiabatic electrons, and the other with kinetic electrons.

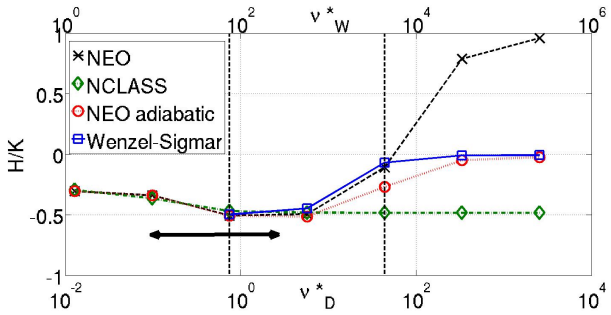

Figure 1: H/K versus D and W collisionalities. Wenzel-Sigmar formulation equations (5) and (6) (solid line squares) NCLASS (diamonds) NEO kinetic electrons (dashed line and crosses) and NEO with adiabatic electrons (dot line and circles). The arrow shows JET core values range. Z=34, $\alpha = 1,2.10^{-3}$, $n_D = 10^{19} \rightarrow 3.10^{24}$

Figure 1 can be divided in three zones, separated by vertical dashed lines. Below $\nu_D^* = 0.5$ in zone n°1, deuterium is in the banana regime and W is in plateau. When $0.5 < \nu_D^* < 50$ in zone n°2, W is in Pfirsch-Schlüter regime and D is in banana/plateau regime. Above $\nu_D^* > 50$ in zone n°3, both species are in Pfirsch-Schlüter regime. Core range values for the JET-ILW case studied and described in section 3 covers zones one and two, with W in plateau/Pfirsch-Schlüter, and D in banana/plateau (see figure 3). One can start with the first zone : D banana and W plateau. When the W is in plateau Wenzel-Sigmar is not applicable. In this zone, both NEO and NCLASS agree very well with each other. In the second zone, the H/K value derived in Wenzel-Sigmar in [21] equals -1/2, NEO and NCLASS first converge towards -1/2. But as ν_D^* enters the third zone, NCLASS remains at -0.5 while H/K from [21] and both NEO curves move away from -0.5. It means that when D and W go deep in plateau, NCLASS is no longer an adequate model. In the third zone both species are in Pfirsch-Schlüter : in this configuration, according to [23] H/K derived in [21] tends to zero. NEO curve with adiabatic electrons goes to zero, but the NCLASS curve remains at -0.5, and NEO with kinetic electrons goes up to 1. NCLASS behavior comes from the fact that it uses a collision operator which does not include energy scattering, which makes it non-relevant with D in Pfirsch-Schlüter. NEO with kinetic electrons differs from the adiabatic electron case due to the electron coupling. Indeed, at low impurity density, the electron collision frequency with the main ions (i.e. ν_{eD}) can become non-neglibible compared with impurity collisional coupling with the main ions (i.e. ν_{DW}). This explains the difference betwen kinetic and adiabatic electron NEO runs. NEO with kinetic electrons is the most physical result. Nonetheless one cannot use H/K=-1/2 in the experimentally relevant range (zone 1 and 2), but NCLASS shows to be reliable enough. However the results showed here are not applicable in the pedestal region.

Two conclusions can be made out of this study of H/K term over Deuterium collisionality. First, typical tokamak collisionality ranges values cover a zone where |H/K| can be lower than 0.5. It means that keeping the numerical value in equation (1) is not adequate to describe experimental plasmas. Secondly, NEO and NCLASS give the same results within the experimental parameter range. Therefore the combination of NCLASS with P_A and P_B formula (equations (1) (2) (3) and [12]) will be compared to NEO with poloidal asymmetries.

Therefore, we assume a generalisation of equation (1) as follows :

$$\frac{R\langle\Gamma_Z^{neo}\rangle}{\langle n_Z\rangle} = q^2 D_c Z\left[\left(K\frac{1}{Z}\frac{R}{L_{nZ}} - K\frac{R}{L_{ni}} - H\frac{R}{L_{Ti}}\right)P_A^{model} - H_0 f_C P_B^{model}\frac{R}{L_{Ti}}\right] \tag{7}$$

In the limit of main ion in banana regime and W in the trace limit and Pfirsch-Schlüter regime, K=1, H=-0.5 and $H_0 = 0.33$ and equation (1) is recovered. The numerical value 0.33 associated with P_B term in equation (1) is also valid only for W in Pfirsch-Schlüter. But as shown later in figure 3 W is mainly in plateau for the studied JET pulse. Therefore the 0.33 value is generalized to an H_0 numerical term that will be defined based on the comparison between NEO results and analytical formulation.

2. *Isolating P_A and P_B terms from NEO outputs*

In order to explore the validity of equation (7), one needs to isolate the transport coefficients from NEO outputs, and then deduce P_A and P_B terms calculated with NEO and compare them to their theoretical expressions (equations (2) and (3)). For clarity, equation (7) is re-written : the idea is to gather the terms respectively in front of densities and temperature gradients. The general version of the flux equation, written in equation (8) below is the starting point. The impurity flux is expressed as the sum of a diffusion term and a convective part. The diffusion coefficient is D_{asym}^{model} and the convection velocity coefficient is identified as V_{asym}^{model}. The index asym stands for asymmetric, i.e accounting for the effects of poloidal asymmetries. "model" means that the coefficients are based on analytical derivation.

$$\left\langle\Gamma_{asym,Z}^{model}\right\rangle = \frac{D_{asym}^{model} n_Z}{R}\left(\frac{R}{L_{nZ}} + \frac{V_{asym}^{model} R}{D_{asym}^{model}}\right) \tag{8}$$

with the pinch velocity term defined as

$$V_{asym}^{model} R = V_{N,asym}^{model}\frac{R}{L_{ni}} + V_{T,asym}^{model}\frac{R}{L_{Ti}} \tag{9}$$

We define $V_{N,asym}^{model}$ and $V_{T,asym}^{model}$ as the convection velocities respectively proportional to $\frac{R}{L_{ni}}$ and $\frac{R}{L_{Ti}}$:

$$V_{N,asym}^{model} = D_{asym}^{model} C_{N,asym}^{model}\frac{1}{L_{ni}} \tag{10}$$

$$V_{T,asym}^{model} = D_{asym}^{model} C_{T,asym}^{model}\frac{1}{L_{Ti}} \tag{11}$$

By identification with equation (7) the coefficients D_{asym}^{model}, $C_{N,asym}^{model}$and $C_{T,asym}^{model}$can be written as follows :

$$D_{asym}^{model} = q^2 D_c K P_A^{model} = D_{sym}^{model} P_A^{model} \tag{12}$$

$$C_{N,asym}^{model} = C_{N,sym}^{model} = -Z \tag{13}$$

$$C_{T,asym}^{model} = -Z\left(\frac{H}{K} + \frac{H_0 f_C P_B^{model}}{K P_A^{model}}\right) = C_{T,sym}^{model} - \frac{Z H_0 f_C P_B^{model}}{K P_A^{model}} \tag{14}$$

In equation (14) f_c is the fraction of circulating particles, defined as $f_c = \frac{3\langle B^2\rangle}{4}\int_0^{\lambda_c}\frac{\lambda d\lambda}{\left(\sqrt{1-\lambda B}\right)}$with λ the pitch-angle variable and $\lambda_c = \frac{1}{B_{max}}$.$f_c$ is calculated by NEO and used later in the comparison. To recover the transport coefficients in absence of poloidal asymmetries : D_{sym}^{model}, $C_{N,sym}^{model}$and $C_{T,sym}^{model}$one just needs to set $P_A = 1$ and $P_B = 0$ in equations (12)-(14).

Next we compute the coefficients (10)-(12) from NEO results. The NEO inputs and outputs that are relevant in our simulations are listed in table 1. NEO inputs are defined at the outboard midplane, noted as $(.)_0$in table 1.

Inputs	Outputs
$(\frac{R}{L_{ni}})_0$, $(\frac{R}{L_{Ti}})_0$, $(\frac{R}{L_{nZ}})_0$, $n_{W,0}/n_{i,0}$	$\Gamma^{model}_{asym,Z}$, $\Gamma^{model}_{sym,Z}$, f_c

Table I: NEO relevant inputs and outputs used for the simulations

Unless stated otherwise, simulations are made with three species, deuterium, electrons and tungsten. NEO equilibrium coefficients come from the EFIT numerical equilibrium of JET-ILW pulse 85308 at 10.35s. To isolate the diffusion coefficient computed by NEO D^{NEO}_{asym}, two NEO runs are needed : they are called runs 1 and 2. They share the same inputs, except for the impurity density gradient $(\frac{R}{L_{nZ}})_0$. To make NEO definition consistent with the gradient of the flux surface average density $\frac{R}{L_{nZ}}$ used in equation (1), the transformation $(\frac{R}{L_{nZ}})_0 = \frac{R}{L_{nZ}}\frac{\langle n_Z\rangle}{n_{Z,0}}$ is used. Indeed equation (1) uses the average gradient length as defined in [20], therefore a correction factor $\frac{\langle n_Z\rangle}{n_{Z,0}}$was added to the NEO gradient length defined at the outboard midplane. $\langle n_Z\rangle$is the W flux surface averaged density, and $n_{Z,0}$ is the W density at the outboard midplane.Γ_1 is the output flux associated with the input $\frac{R}{L_{nZ}} = 2$, noted as $(\frac{R}{L_{nZ}})_1$. Γ_2 is associated with $\frac{R}{L_{nZ}} = 5$, noted as $(\frac{R}{L_{nZ}})_2$. D^{NEO}_{asym} is then calculated as shown in equation (15) :

$$D^{NEO}_{asym} = \frac{R}{\langle n_Z\rangle}\frac{\Gamma_2 - \Gamma_1}{(\frac{R}{L_{nZ}})_2 - (\frac{R}{L_{nZ}})_1} \tag{15}$$

We assume that the description of equation (10) is correct, so that $V^{NEO}_{N,asym} = -ZD^{NEO}_{asym}\frac{1}{L_{ni}}$.

To isolate $V^{NEO}_{T,asym}$, an extra NEO run is needed, with a different main ion temperature gradient compared with run 1. Γ_1 is the output flux associated with the input $(\frac{R}{L_{T_i}})_1 = 1$, Γ_3 is associated with $(\frac{R}{L_{T_i}})_3 = 0$. It gives equation (16) :

$$V^{NEO}_{T,asym} = \frac{R}{\langle n_Z\rangle}\frac{\Gamma_1 - \Gamma_3}{(\frac{R}{L_{Ti}})_1 - (\frac{R}{L_{Ti}})_3}\frac{1}{L_{Ti}} \tag{16}$$

In total, to compute transport coefficients with poloidal asymmetries$D^{NEO}_{asym}$and $V^{NEO}_{T,asym}$, and coefficients without poloidal asymmetries,$D^{NEO}_{sym}$and $V^{NEO}_{T,sym}$, 6 NEO runs are needed.

Since the P^{model}_Ageometry coefficient is equivalent to :

$$P^{model}_A = \frac{D^{model}_{asym}}{D^{model}_{sym}} \tag{17}$$

And assuming that equation (7) is an accurate description of NEO results, we define P^{NEO}_A as follows :

$$P^{NEO}_A = \frac{D^{NEO}_{asym}}{D^{NEO}_{sym}} \tag{18}$$

Now we have isolated P^{NEO}_A from NEO coefficients, we need to do the same with P^{NEO}_B. However, isolating H_0P_B alone from NEO transport coefficients is not possible using NEO coefficients (equations (15)-(16)). Therefore the term Q^{NEO}_B is defined in equation (20), for it is the simplest coefficient including H_0P_B that can be isolated. Assuming that equation (7) is a good description of NEO results, Q^{model}_B is defined, isolated using analytical coefficients as shown in equation (19).

$$Q^{model}_B = -\frac{H_0 f_C P^{model}_B}{H} = \frac{V^{model}_{T,sym}P^{model}_A - V^{model}_{T,asym}}{V^{model}_{T,sym}} \tag{19}$$

$$Q^{NEO}_B = \frac{V^{NEO}_{T,sym}\frac{D^{NEO}_{asym}}{D^{NEO}_{sym}} - V^{NEO}_{T,asym}}{V^{NEO}_{T,sym}} \tag{20}$$

Now we compare the model built from the generalization equation (7) of the analytical formula with NEO.

III. POLOIDAL ASYMMETRIES IMPACT ON NEOCLASSICAL TRANSPORT : NEO VS FORMULA

In this section P_A^{NEO} and Q_B^{NEO} are compared with P_A^{model} and Q_B^{model} for a given case of JET-ILW plasma profiles. Transport coefficients are then reconstructed with a combination of NCLASS runs and geometrical P_A^{model} and P_B^{model} and compared with NEO isolated transport coefficients.

A. Selected JET pulse description and collisionality profiles

This section focuses on the first test of the robustness of the model. The comparison between NEO and analytical P_A^{model} and Q_B^{model} is based on JET-ILW parameters from the baseline H-mode shot 85308 ($I_P = 2.5MA$ and B=2.7T), also presented in [6]. The heating power of this discharge is 19.1 MW of NBI. W, Be, Hydrogen and Helium are present in the NEO simulations. The W concentration is arbitrarily chosen so that $n_W/n_i = 10^{-5}$ and W remains a trace specie. Other dimensionless quantities are shown in table 2. Figure 2 shows the main JET based input profiles, and figure 3 shows the collisionalities calculated with these inputs. Table 2 gives the main quantities that are used for NEO runs at three radial locations, with r/a defined as the ratio of the mid-plane averaged minor radius r, to the mid-plane minor radius r at the last closed flux surface a. In this section, unless specified otherwise, NEO resolution is the following : 21 theta poloidal gridpoints, 19 extensions in pitch-angle Legendre polynomial, and 10 energy polynomials. These resolutions were checked to be sufficient at the extrema of our scans.

r/a	$R/L_{T_D} = R/L_{T_e}$	R/L_{n_e}	Z	Z_{eff}	q	n_W/n_i	M_D	M_W
0.1	2.4	1	44	1.39	0.9	10^{-5}	0.19	1.82
0.4	5.2	1.4	38	1.37	1	10^{-5}	0.18	1.78
0.8	10.4	2.8	26	1.29	2	10^{-5}	0.17	1.66

Table II: JET data main inputs. Pulse 85308 time averaged over 10.35s-10.85s

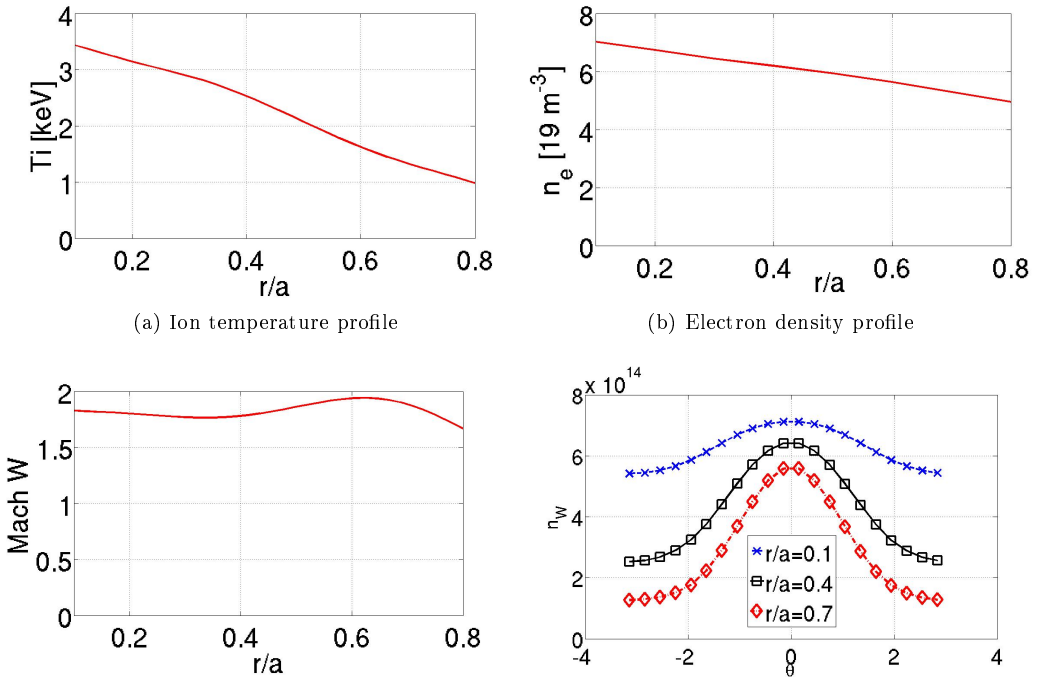

(a) Ion temperature profile

(b) Electron density profile

(c) Impurity (here Tungsten W) Mach number

(d) W distribution vs the poloidal angle θ from NEO simulations for r/a=0.1 (blue,cross) 0.4 (dark, square) 0.8 (red, diamond)

Figure 2: Input profiles from JET 85308 baseline H-mode shot ($I_P = 2.5MA$ and B=2.7T) for simulated timeslice (averaged over t=10.35s-10.85s). Experimental data and error bars can be found in [6].

The Mach number is defined as $M=\sqrt{\frac{m\omega^2 R^2}{2T}}$ where m is the mass of the considered species, R is the major radius, T the temperature and ω is the angular frequency. Mach number from figure 2c) is computed with NEO based on experimental angular frequency and temperature.

Collisionality parameter is defined as $\nu^* = \frac{qR\nu}{v_{th}\epsilon^{3/2}}$, with ν the collision frequency defined as $\nu_{12} = \frac{1}{3(2\pi)^{3/2}} \frac{n_2 e_1^2 e_2^2 ln\Lambda}{\varepsilon_0{}^2 m_1^{1/2} T_1^{3/2}}$ (ν_{eD} for $\nu_D^*$and ν_{WD} for ν_W^*).

Figure 2d) shows that poloidal asymmetries are stronger at the edge. This comes from the R dependency in the expression of the W density presented in [6] and re-written in equation (21):

$$n_W(\theta) = n_0 \exp(-\frac{eZ\phi(\theta)}{T_{/\!/}} + \frac{m\Omega^2(R(\theta)^2 - R_0^2)}{2T_{/\!/}}) \tag{21}$$

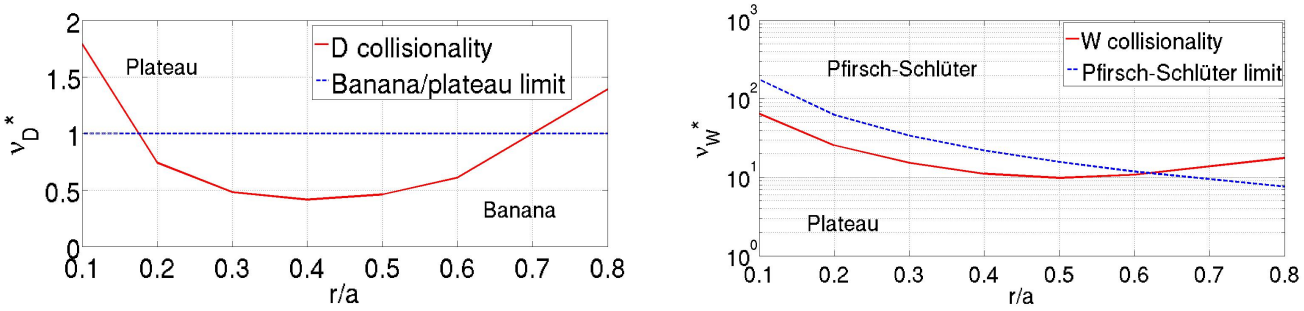

(a) D collisionality

(b) W collisionality

Figure 3: D and W collisionalities calculated from JET 85308 in figure 2.

Figure 3a) illustrates the D collisionality and the limit banana-plateau regime. Deuterium is plateau in the core and at the edge, and banana elsewhere. On figure 3b), the dashed line corresponds to the limit above which W reaches the Pfirsch-Schlüter regime. One can see that W is in Pfirsch-Schlüter regime only at r/a>0.6. Therefore there is no radial range where both species are in the regimes (W trace and Pfirsch-Schlüter, D banana) where the Angioni and Helander formula strictly applies. In the next section we compare P_A^{model} and Q_B^{model} with NEO coefficients and we study the impact of the theoretical assumptions.

B. P_A and Q_B terms

P_A and Q_B terms were isolated as explained in the previous section. On figure 4, H corresponds to the Wenzel-Sigmar formulation from equation (4). For the studied JET-ILW case, H stays very close to -0,5.

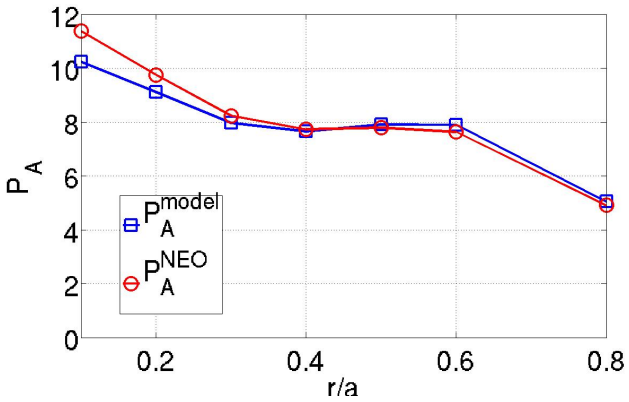

(a) Asymmetry pinch enhancement

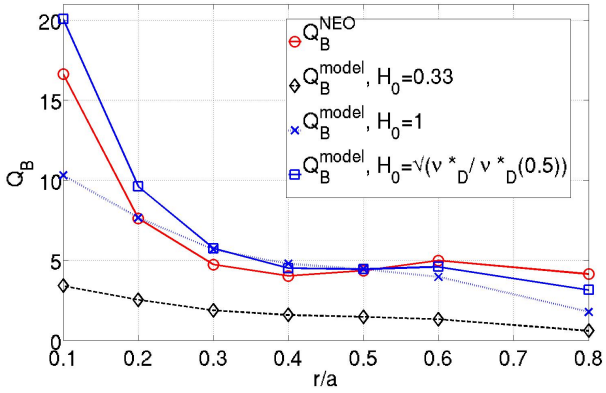

(b) Temperature screening reduction

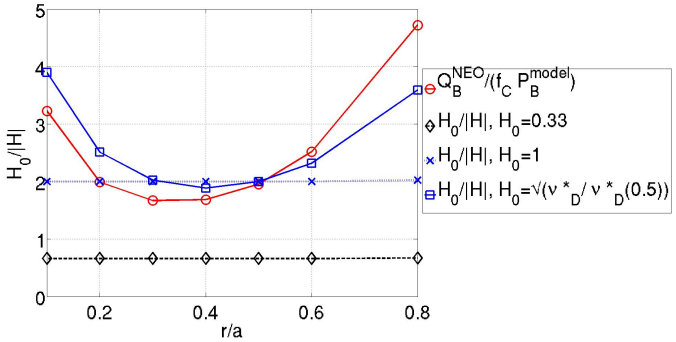

(c) Ratio of temperature screening coefficients

Figure 4: Comparison of NEO results and model results for JET data pulse n°85308

On figure 4a) one can see that globally P_A^{model} shows a good agreement with NEO, which is very encouraging because, as seen in figure 3), not all the assumptions of the analytical derivation are well fulfilled in this pulse. However, one can note that at $r/a = 0.1 - 0.3$, P_A^{model} underestimates P_A^{NEO}. Figure 4b) shows Q_B^{NEO} compared with different Q_B^{model} combinations, each with a different H_0 formulation. Figure 4c) shows the numerical value of $H_0/|H|$ isolated : Q_B^{NEO} is divided by $f_C P_B^{model}$, assuming that equation (7) is an accurate description of NEO results. $|H|$ corresponds ton Wenzel-Sigmar coefficient froml equation (6). On figure 4b) one can see that Q_B^{model} with $H_0 = 0.33$ (dashed line and diamond) is well below Q_B^{NEO} (circles and solid line). Q_B^{model} with $H_0 = 1$ (crosses and dot line) seems to be a better approximation, but at low r/a the fit can be improved. The best fit out of the three H_0 formulations presented here seems to be $H_0 = \sqrt{\nu_D*/\nu_D*(0.5)}$, with $\nu*_D\,(0.5)$ the value of D main ion collisionality at r/a=0,5 (solid line and squares). The collisionality dependence allows to simultaneously reproduce the increase of $H_0/|H|$ in the center and towards the last closed flux surface, shown on figure 4c). The normalisation of main ion collisionality at r/a=0,5 was chosen because of the excellent agreement between Q_B^{NEO} and Q_B^{model}. Physics based motivation is presently missing. Indeed, according to [15], the 0.33 value was calculated with a simplified collision operator and remains valid only with W in Pfirsch-Schlüter regime and D in banana regime, for large temperature and density gradients. One can see that $H_0 = 1$ is a better fit to the numerical results than 0.33, but it mismatches at small r/a and r/a>0.6. The H_0 formulation depending on the collisionality gives a better match. However according to the Appendix A, the collisionality dependent H_0 does not appear to be universal, therefore a more physics based formulation for H_0 is required instead of an adjusted formulation depending on the normalization value.

To summarize, there is no radial range where both species are in the regimes (W trace and Pfirsch-Schlüter, D banana) where the Angioni and Helander formula strictly applies. However analytical P_A^{model} and Q_B^{model} show a very good agreement with NEO coefficients, provided a collisionality dependence is introduced in H_0. In order to study the validity of the formula out of its limits, and try to quantify its reliability, two main assumptions of the formula are studied in Appendix A and B : the collisionality and the Mach number dependencies. In Appendix A the characteristics of the W are artificially modified, in order to make it Pfirsch-Schlüter while D is in banana. This is done by increasing the W charge number or its density, while keeping the trace limit. The conclusion of this study is that

having D in banana regime is an essential assumption to get an acceptable agreement between NEO and the model. Once this assumption is fulfilled, the W regime becomes less critical. For the other cases, especially both species in plateau, the theoretical formula does not give a good fit : one will have to use NEO with poloidal asymmetries. Therefore the departure of P_A at low r/a of the JET-ILW case, on figure 4a), is likely due to having D and W in plateau where the analytical formula is not reproducing well NEO. Also the collisionality dependent H_0 formulation appears to probably be specific to the case studied here and cannot be generalized. In Appendix B we study the impact of W and D Mach numbers on the analytical formula. The results show that for W Mach numbers >2 P_A^{model} over estimates NEO results (up to 50%), impacting also Q_B^{model} term. But for this JET-ILW case, as shown on figure 2c) W Mach number is low enough so that analytical coefficients can be used.

C. Reconstruction of transport coefficients using NCLASS

To complete the test of the validity of the model, one can compare NEO coefficients from equations (15)-(16) with a combination of NCLASS runs and geometrical P_A^{model} and P_B^{model} from equations (2) and (3). NCLASS inside JETTO provides a factor 1100 speedup compared with NEO because it is a fluid-moment based model, solving a lower dimensionality problem, while NEO solves exactly the drift kinetic equation. Moreover, NCLASS uses a simple collision operator, which saves time compared to NEO especially with multi-species cases, like the JET-ILW pulse used here.

For clarity, the three transport coefficients are presented as they would be used in a transport code : the diffusion term, defined in equation (12); the main ion gradient pinch velocity term, defined in equation (10); and the temperature screening term, defined in equation (11). But instead of using the analytical expressions from equations (10)-(12), we use NCLASS poloidally symmetric transport coefficients D_{sym}^{NCLASS}, $V_{N,sym}^{NCLASS}$ and $V_{T,sym}^{NCLASS}$, obtained by using the same procedure shown in equations (15)-(16). Therefore we define, in equations (22)-(24), coefficients that combine NCLASS poloidally coefficients and analytical P_A and P_B : $D_{asym}^{NCLASS,model}$, $V_{N,asym}^{NCLASS,model}$ and $V_{T,asym}^{NCLASS,model}$.

$$D_{asym}^{NCLASS,model} = D_{sym}^{NCLASS} P_A^{model} \tag{22}$$

$$V_{N,asym}^{NCLASS,model} = Z D_{sym}^{NCLASS} P_A^{model} \frac{R}{L_{ni}} \tag{23}$$

$$V_{T,asym}^{NCLASS,model} = V_{T,sym}^{NCLASS} \left[P_A^{model} + \frac{H_0 f_C P_B^{model}}{H} \right] \tag{24}$$

For the comparison between NCLASS and NEO we also introduce transport coefficients which are a combination of NEO poloidally symmetric coefficients associated with P_A^{model} and P_B^{model} , defined as follows :

$$D_{asym}^{NEO,model} = D_{sym}^{NEO} P_A^{model} \tag{25}$$

$$V_{N,asym}^{NEO,model} = Z D_{sym}^{NEO} P_A^{model} \frac{R}{L_{ni}} \tag{26}$$

$$V_{T,asym}^{NEO,model} = V_{T,sym}^{NEO} \left[P_A^{model} + \frac{H_0 f_C P_B^{model}}{H} \right] \tag{27}$$

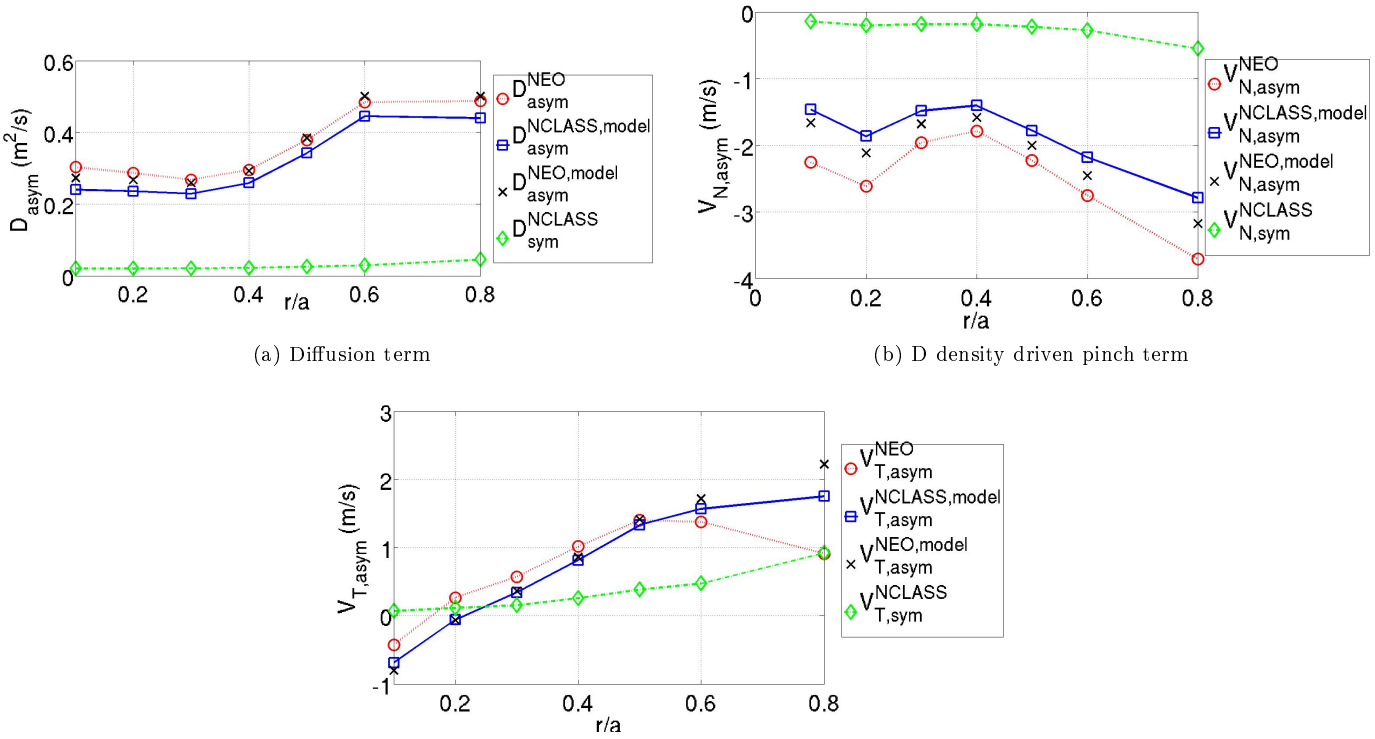

(a) Diffusion term

(b) D density driven pinch term

(c) Temperature screening term

Figure 5: Reconstruction of W transport coefficients : comparison between NEO and NCLASS+correction factors

First of all, one can notice on figures 5 that NCLASS alone (dash-dot line and diamonds) is totally wrong for all transport coefficients. On the contrary NCLASS combined with P_A^{model} and P_B^{model} is very close to NEO coefficients, both symmetric and asymmetric, while obtained 1100 times faster. Indeed NEO runs take the same time, with or without asymmetry.

Regarding the diffusion term (figure 5a)), $D_{sym}^{NCLASS} \times P_A^{model}$ (squares and full line) is lower than both NEO-only diffusion coefficient (circles and dotted line), and NEO symmetric combined with P_A^{model} (crosses). The difference in collision operator between NEO and NCLASS explains the gap between $D_{sym}^{NCLASS} \times P_A^{model}$ and NEO symmetric combined with P_A^{model} . Finally the difference between NEO symmetric combined with P_A^{model} and NEO-only diffusion coefficient comes from the difference between P_A^{model} and P_A^{NEO}on figure 4. We mostly want to see how $D_{sym}^{NCLASS} \times P_A^{model}$ compares with NEO-only diffusion coefficient and despite we recover the difference between P_A^{model} and P_A^{NEO}on figure 4, both coefficients remain comparable.

The fit on the D density driven pinch term on figure 5)b) shows a similar trend : NCLASS combined with analytical P_A^{model} and Q_B^{model} is lower than NEO-only coefficient. One can notice that this term is one order of magnitude bigger than the diffusion term in figure 5a), due to the W charge factor.

Concerning the temperature screening term on figure 5c) we use $H_0 = \sqrt{\nu_{D^*}/\nu_{*D}(0.5)}$ as it seems to be the best adjustment for this case. On figure 5c), there is a sign change at low epsilon, coming from H_0 and H compensating each other. The agreement between NEO and NCLASS combined with analytical P_A^{model} and Q_B^{model} is very good except for the last point at r/a=0.8. However one can notice that the temperature asymmetry screening term is two times weaker than the D density driven pinch contribution to the W flux. Overall, the combination of NCLASS and theoretical P_A^{model} and Q_B^{model} reproduces correctly, within 35%, the NEO results.

The last step is to test the combination NCLASS + geometric P_A^{model} and Q_B^{model} inside JET transport solver, JETTO. The goal is to compare the flux outputs, but also the computation time between the combination of NCLASS with P_A^{model} and Q_B^{model} and full NEO with poloidal asymmetries.

IV. APPLICATION IN JETTO

P_A^{model} and Q_B^{model} equations are implemented in the JET integrated modeling platform JETTO [11]. JETTO is coupled with NCLASS and NEO, but also with the impurity module SANCO [24], that calculates impurity profiles and the amount of radiation produced. We compare on figure 6 the W profile calculated with NEO inside JETTO, and the W profile calculated using NCLASS associated with geometric P_A^{model} and Q_B^{model}. The simulations are performed over 0,5s so that all codes are converged, with one set of interpretive background profiles. Only W density profile is evolving. The input profiles used in JETTO are based on the JET pulse 85308 illustrated on figure 2. In order to test the neoclassical W transport, the W turbulent transport is artificially reduced. NCLASS simulations with P_A^{model} and Q_B^{model} ran on average 1100 times faster compared with NEO simulations.

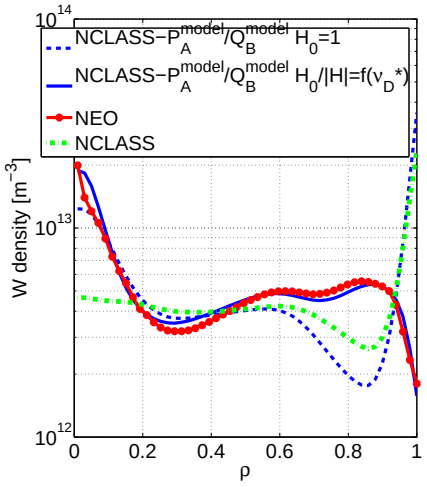

Figure 6: W density profile depending on ρ : comparison between NEO and NCLASS $+P_A^{model}$ / P_B^{model} inside JETTO based on JET case 85308

On figure 6, the predicted W density profiles by NEO and by NCLASS$+P_A^{model}$ / Q_B^{model} model are compared. One can see that within ρ=0.5 NEO (full line and circles) and NCLASS$+P_A^{model}$ / Q_B^{model} with H_0 depending on ν_D* (full line) are very close. The agreement of NEO with and NCLASS$+P_A^{model}$ / Q_B^{model} with $H_0/|H| = 2$ (dashed line) is also very good within ρ=0.5. NCLASS (dashed and dotted line) does not capture the W core density peaking. For ρ larger than 0.5 up to the pedestal region, the curves split in two groups : NCLASS$+P_A^{model}$ / Q_B^{model} with H_0 depending on ν_D* stays in very good agreement with NEO. However in this region NCLASS alone and NCLASS$+P_A^{model}$ / Q_B^{model} with $H_0/|H| = 2$ both underestimate NEO results. This might be explained by the fact that in this region W enters the Pfirsch-Schlüter regime and Deuterium enters plateau regime. According to figure 1) NCLASS and NEO start to diverge in that region and that may lead to the discrepancy seen on figure 6. It is possible that the collisionality dependent $H_0/|H|$ compensates this effect so that NCLASS combined with this H_0 formulation still agrees with NEO. In the pedestal region the study made in section II.b) does not apply. NCLASS alone and NCLASS$+P_A^{model}$ / Q_B^{model} with $H_0/|H| = 2$ both present an unrealistic peaking at the boundary. NCLASS$+P_A^{model}$ / Q_B^{model} with H_0 depending on ν_D* keeps its very good agreement with NEO. Therefore a H_0 increase with ν_D* increasing seems to be a key ingredient to predict the W profile. The underlying physics still requires to be investigated.

To summarize, NCLASS associated with the equations P_A^{model} and Q_B^{model} allows to reproduce the W density predicted by NEO in JETTO, while being 1100 times faster. The choice of the collisionality dependency of H_0 formulation was proved to be crucial to reproduce of NEO results.

V. CONCLUSIONS

Due to its large mass and charge, Tungsten neoclassical transport can be enhanced significantly by poloidal asymmetries [16]. Poloidal asymmetries are produced by the centrifugal force in presence of NBI [14–17, 25] and/or by RF heating [8, 26, 27]. In some JET cases, the enhancement can reach an order of magnitude (first established in [5] and continued in [6, 20]). It is therefore essential to take poloidal asymmetries into account in integrated modeling. The effect of poloidal asymmetries are captured by the neoclassical code NEO. However, NEO leads to significant computational expense in integrated modelling applications. The goal of this paper was to determine if it was feasible to combine geometric analytical terms describing the effect of poloidal asymmetries on W flux, with a simpler neoclassical code, NCLASS, in order to produce results similar to the ones obtained with NEO.

The results show that the assumptions of the analytical formula [16] are hardly fulfilled simultaneously, especially for the collisionality constraints. Indeed, the analytical model required the D to be in the banana regime and the W in the PS regime, whereas experimentally when D is in the banana regime the W is in the plateau regime and when W is in the PS regime, the D is in the plateau regime. Nonetheless the robustness of the analytical formulation was explored outside of the collisionality regimes in which it was derived. Towards the magnetic axis, having D and W collisionalities in plateau leads to slightly under estimated convection enhancement factor, which sightly impacts the reconstruction of the transport coefficients. As long as the D is in the banana regime, the analytic formula can be applied even with a W out of the PS regime. If the D is in the plateau regime, then the analytical formulation is only applicable for W in the PS regime. Outside of these regimes, the analytical formula cannot be used. Also when D and W go deep in plateau, NCLASS is no longer an adequate model. Nonetheless the applicability range is large. For future devices such as ITER and DEMO, the validity range of this model is even wider, since the main ions will be in the banana regime in a greater radial extent compared to present day machines. Moreover in such devices neoclassical transport is expected to be much less dominant than in present devices with beneficial effects on W behavior, as presented in [28]. The results obtained in this paper are highly encouraging for application of the model in integrated modelling applications, saving significant computational time in W-transport simulations in the presence of poloidal asymmetries, compared to full NEO calculations. The analytical formula has been optimized to match better NEO by accounting for a collisionality dependence in the correction factor of the temperature gradient convection part due to poloidal asymetries. This collisionality dependence requires additional work to be explained by neoclassical theory. Finally for very strong poloidal asymmetries in this regime, geometric convection enhancement factor overestimates NEO results (up to 50%), impacting also temperature screening term.

A neoclassical code, NCLASS, has hence be coupled to the analytical geometric formula and integrated in JETTO. The test on a JET based parameters is very encouraging and show that the W density profile is well predicted by the simplified model while saving a factor 1100 computing time.

Appendix A: Collisionality dependence

The first parameter studied is the collisionality dependence. Both D collisionality and W collisionality regimes are important for the analytical derivation. The goal of this section is to start from collisionality limits required for the analytical model and move away from them, and see how well our model behaves.

D collisionality is scanned by varying the D density. Two cases are explored : one with W in plateau (closer to the reality) and one with W in Pfirsch-Schlüter (closer to theoretical assumptions). In both cases, the D density varies in order to change the collisionality regime. Since W density is fixed, the alpha parameter $\alpha = \frac{Z_Z^2 n_Z}{n_i}$ varies with the D density such that the trace impurity condition is not valid everywhere. It is not possible to satisfy all the assumptions of the theory simultaneously.

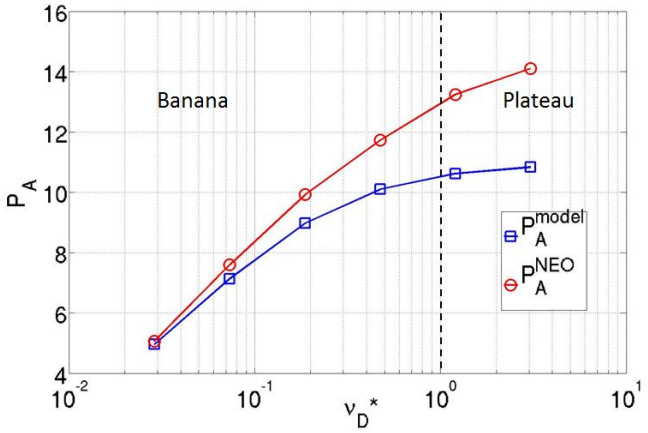

(a) W in plateau. Vertical dashed lines define the JET-ILW 85308 values range. $\alpha = 1.4 \rightarrow 0.2$ for $\nu* = 2.10^{-2} \rightarrow 3$

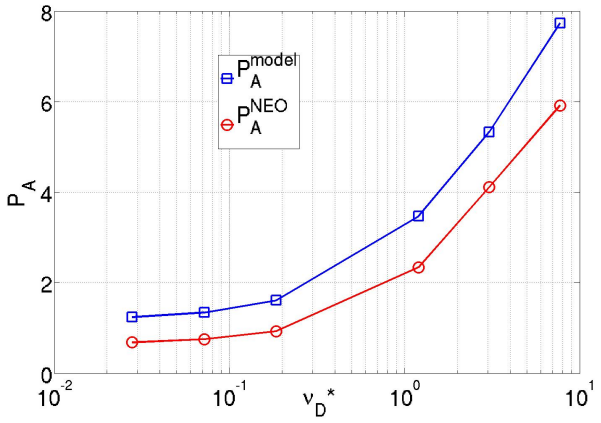

(b) W in Pfirsch-Schlüter. $\alpha : 140 \rightarrow 2$for $\nu* = 2.10^{-2} \rightarrow 3$

Figure 7: Asymmetry enhancement depending on D collisionality and α. JET data pulse n°85308, r/a=0.1 data from table 1. Z=1,39

Figure 7a) illustrates the D collisionality scan, for P_A, with W in plateau regime. When D is in deep banana regime, P_A^{NEO} and P_A^{model} agree very well. But the formula starts to mismatch NEO even while D is still in the banana with ν_D^*<1. The further D departs from banana regime the bigger is the discrepancy with respect to P_A^{model}. This shows the importance of having D in banana while W is in plateau regime. It also means that the formula is reliable even if W is not in Pfirsch-Schlüter regime, as long as D is in banana. On figure 7b) one can see again a D collisionality scan for P_A, with W in Pfirsch-Schlüter regime. The fit is sightly better with D in banana regime, but even when D goes deeper in plateau regime the error is about 15%, which is comparable with the error on figure 7a), with D in plateau. It means that having W in plateau or in Pfirsch-Schlüter does not strongly impact on P_A behavior, which is a bit surprising. However, one can also notice that P_A values are much smaller with W in Pfirsch-Schlüter because of the increasing of W density. Forcing W in Pfirsch-Schlüter also impacts the trace limit assumption, which could explain why the fit is not better with W in Pfirsch-Schlüter. As already observed when computing P_A and Q_B on the JET-ILW pulse case, fulfilling the collisionality assumptions simultaneously is not mandatory to have an accurate estimate of P_A.

One can do the same exercise for Q_B. Again the deuterium collisionality varies while fixing W density so W can stay in one collisionality regime.

Figure 8a) illustrates the D collisionality scan, for Q_B, with W in plateau regime, with H_0=1 and H_0 as a function of ν_D^*since it is believed to be the best approximation, according to section III. One can see that no H_0 formulation is a match for all D collisionalities. H_0=1 overestimates Q_B at low collisionalities and underestimates it at higher collisionality. H_0 as a function of ν_D^* shows a very different trend compared with Q_B^{NEO}, showing that this H_0 formulation is probably specific to the case studied here and cannot be generalized. The agreement between Q_B^{NEO} and Q_B^{model} with H_0=1 is acceptable with D in banana regime, but once D is in plateau the three curves diverge. It means that having D in banana regime is essential to keep an acceptable agreement with NEO, since we don't have an H_0 formulation robust enough to work in plateau regime. However Q_B is involved only on the temperature screening term, which is smaller than the density gradient component of the convection. Therefore, the final impact on W density might be limited.

On figure 8b), with W in Pfirsch-Schlüter and D in banana, all three curves show a very good agreement on Q_B. However one can notice that forcing W in Pfirsch-Schlüter caused Q_B values to be close to zero when D is in deep banana regime. This explains the strong values of NEO's $\frac{H_0}{|H|}$ on figure 8d) but the discrepancy between the different values of $\frac{H_0}{|H|}$ doesn't prevent a good agreement on Q_B. However when D reaches plateau regime, H_0=1 case keeps a good agreement with NEO while H_0 as a function of ν_D^*case strongly overestimates Q_B. Again having D in banana regime is essential to have an acceptable agreement between NEO and the model.

Figures 8c) and 8d) show the absolute value of $\frac{H_0}{|H|}$, compared with Q_B^{NEO} / $f_C P_B^{model}$.Q_B^{NEO} / $f_C P_B^{model}$ clearly shows a D collisionality dependence but there is not clear trend that could lead to a better formulation for the numerical 0,33.

As a conclusion, one can say that having D in banana is an essential assumption to get an acceptable agreement between NEO and the model. Once this assumption is fulfilled, the W regime becomes less critical. For the other

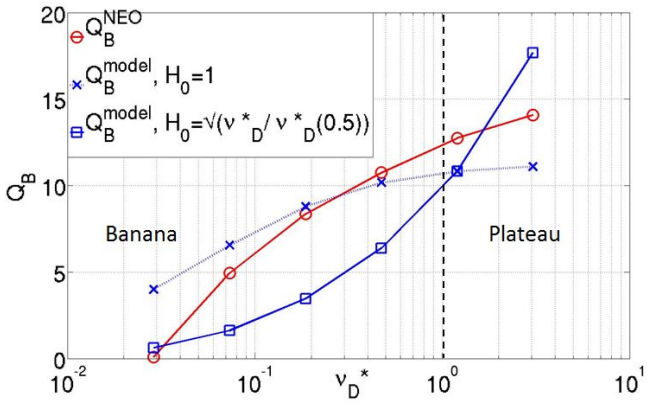

(a) W in plateau. $\alpha : 1.4 \rightarrow 0.2$ for $\nu* = 2.10^{-2} \rightarrow 3$

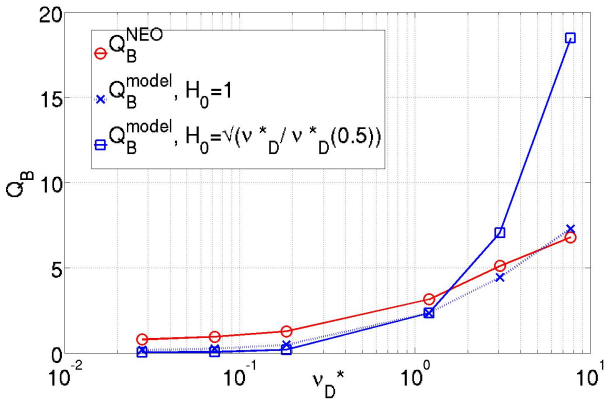

(b) W in Pfirsch-Schlüter. $\alpha : 140 \rightarrow 2$ for $\nu* = 2.10^{-2} \rightarrow 3$

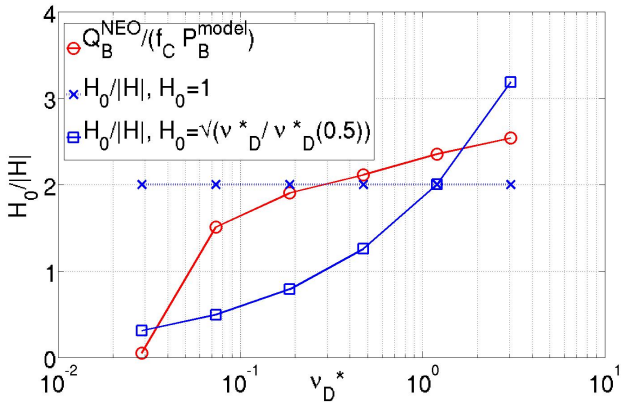

(c) Detail of the temperature screening reduction, in absolute value : W in plateau

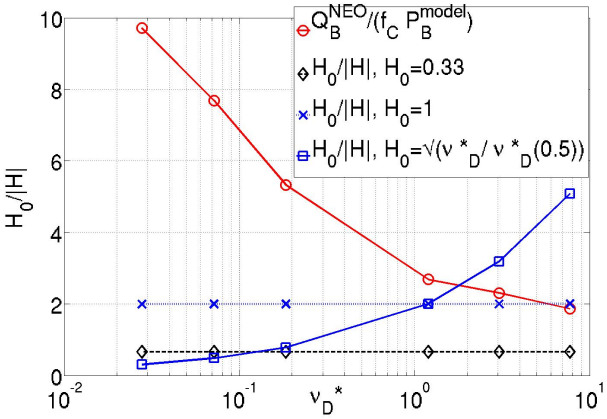

(d) Detail of the temperature screening reduction, in absolute value : W in Pfirsch-Schlüter

Figure 8: Temperature screening reduction term depending on D collisionality and α. JET data shot n°85308, r/a=0.1 table 1

cases, especially both species in plateau, the theoretical formula does not give a good fit : one will have to use NEO with poloidal asymmetries. Therefore the departure of P_A at low r/a of the JET-ILW case, on figure 4a), is likely due to having D and W in plateau where the analytical formula is not reproducing well NEO.

Appendix B: Mach number dependence

Another assumption needs to be studied : the Mach number dependency. Reference [16] specifies that bulk ion Mach number is assumed to be small, ie $M_i \ll 1$ and heavy impurity Mach number $M_Z = O(1)$. W Mach number up to 3 is observed in JET NBI pulses [5], one wants to explore the behavior of P_A and Q_B up to such values.

Figures 9 illustrate such a scan where both W and D Mach numbers are simultaneously varied. M_D remains well below 1 while M_W approaches 3.

One can see that the agreement is very good until $M_Z \approx 2$; above, NEO does not increase as much as geometric terms predict, both for P_A and Q_B terms with both H_0 formulations. In figure 9, another scan of the W Mach number was made, but this time W is placed in the Pfirsch-Schlüter regime. D is still in plateau regime. The goal of this scan is to identify if it is again the collisionality regime that causes the discrepancies on figures 8.

On figure 9 the fits are almost perfect for P_A until$M_Z \approx 2$, slightly worse for P_B but still much better than with W in plateau. It clearly shows that for strong asymmetries, having W in the Pfirsch-Schlüter regime is mandatory in order to have an accurate estimate of P_A and Q_B terms. One can also notice that the H_0 formulation depending

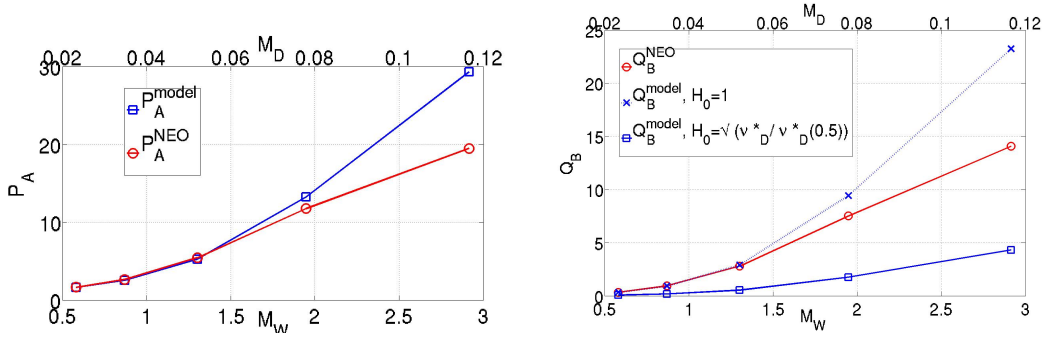

(a) Asymmetry pinch enhancement (b) Temperature screening reduction

Figure 9: P_A andQ_B terms depending on W Mach number. JET data shot n°85308, r/a=0.4 in table 1 except $n_W/n_D = 10^{-6}$. D in banana and W in plateau. For the last two points, NEO resolution increased to 41 theta gridpoints and 39 extensions in Legendre polynomials.

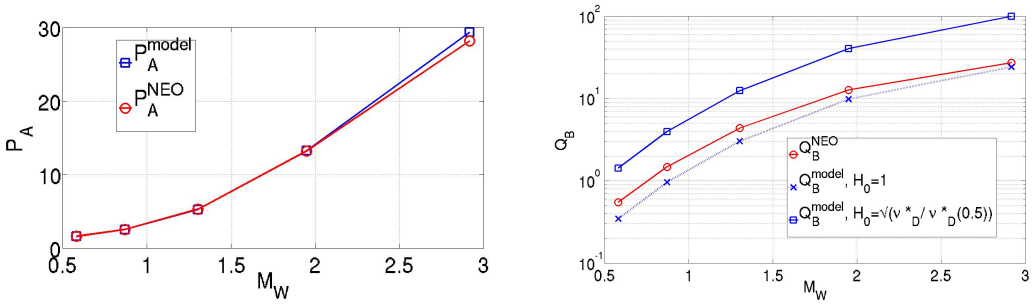

(a) Asymmetry pinch enhancement (b) Temperature screening reduction

Figure 10: P_A and Q_B terms depending on W Mach number. JET data shot n°85308, r/a=0.4 in table 1. D in banana and W in plateau

on ν_D^* strongly overestimates Q_B^{NEO} .It confirms that this H_0 formulation is probably specific to the JET-like case studied here and cannot be generalized.

ACKNOWLEDGMENTS

"This work has been carried out within the framework of the EUROfusion Consortium and has received funding from the Euratom research and training programme 2014-2018 under grant agreement No 633053. The views and opinions expressed herein do not necessarily reflect those of the European Commission."

With the financial support of la Région Provence-Alpes-Côte d'Azur

[1] S. P. Hirshman and D.J. Sigmar. Neoclassical transport of impurities in tokamak plasmas. *Nucl. Fusion*, 1079, 1981.

[2] P. Helander and D.J. Sigmar. *Collisional Transport in Magnetized Plasmas*. 2002.

[3] C. Angioni, L. Carraro, T. Dannert, N. Dubuit, R. Dux, C. Fuchs, X. Garbet, L. Garzotti, C. Giroud, R. Guirlet, F. Jenko, O. J W F Kardaun, L. Lauro-Taroni, P. Mantica, M. Maslov, V. Naulin, R. Neu, A. G. Peeters, G. Pereverzev, M. E. Puiatti, T. Pütterich, J. Stober, M. Valovi, M. Valisa, H. Weisen, and A. Zabolotsky. Particle and impurity transport in the Axial Symmetric Divertor Experiment Upgrade and the Joint European Torus, experimental observations and theoretical understanding. *Physics of Plasmas*, 14(5):1–9, 2007.

[4] T. Fülöp, S. Braun, and I. Pusztai. Impurity transport driven by ion temperature gradient turbulence in tokamak plasmas. *Physics of Plasmas*, 17(6):1–9, 2010.

[5] C Angioni, P Mantica, T Pütterich, M Valisa, M Baruzzo, E A Belli, P Belo, F J Casson, C Challis, P Drewelow, C Giroud, N Hawkes, T C Hender, J Hobirk, T Koskela, L Lauro Taroni, C F Maggi, J Mlynar, T Odstrcil, M L Reinke, M Romanelli, and J E T EFDA Contributors. Tungsten transport in JET H-mode plasmas in hybrid scenario, experimental observations and modelling. *Nuclear Fusion*, 54(8):83028, 2014.

[6] F. J. Casson, C. Angioni, E. A. Belli, R. Bilato, P. Mantica, T. Odstrcil, T. Puetterich, M. Valisa, L. Garzotti, C. Giroud, J. Hobirk, C. F. Maggi, J. Mlynar, M. L. Reinke, JET EFDA Contributors, and ASDEX-Upgrade Team. Theoretical description of heavy impurity transport and its application to the modelling of tungsten in JET and ASDEX Upgrade. *Plasma Physics and Controlled Fusion*, 014031:1–9, 2014.

[7] M L Reinke, I H Hutchinson, and J E Rice. Impact of Impurity Asymmetry Physics on Poloidal Rotation Studies. 2012.

[8] R. Bilato, O. Maj, and C. Angioni. Modelling the influence of temperature anisotropies on poloidal asymmetries of density in the core of rotating plasmas. *Nuclear Fusion*, 54(7):072003, 2014.

[9] E A Belli and J Candy. Kinetic calculation of neoclassical transport including self-consistent electron and impurity dynamics. *Plasma Phys. Control. Fusion*, 50(9):95010, 2008.

[10] E A Belli and J Candy. Full linearized Fokker Planck collisions in neoclassical transport simulations. *Plasma Phys. Control. Fusion*, 54(54):15015–17, 2012.

[11] Michele Romanelli, Gerard Corrigan, Vassili Parail, Sven Wiesen, Roberto Ambrosino, Paula Da, Silva Aresta, Luca Garzotti, Derek Harting, Florian Köchl, Tuomas Koskela, Laura Lauro-taroni, Chiara Marchetto, Massimiliano Mattei, Elina Militello-asp, Maria Filomena, Ferreira Nave, Stanislas Pamela, Antti Salmi, Pär Strand, Association Euratom-fzj, Forschungszentrum Jülich, and D Jülich. JINTRAC : A System of Codes for Integrated Simulation of. 9:1–4, 2014.

[12] W. A. Houlberg, K. C. Shaing, S. P. Hirshman, and M. C. Zarnstorff. Bootstrap current and neoclassical transport in tokamaks of arbitrary collisionality and aspect ratio. *Physics of Plasmas*, 4(9):3230, 1997.

[13] Per Helander. Neoclassical transport in a rotating impure plasma. *Physics of Plasmas*, 5(4):1209–1211, 1998.

[14] M. Romanelli and M. Ottaviani. Effects of density asymmetries on heavy impurity transport in a rotating tokamak plasma. *Plasma Physics and Controlled Fusion*, 40(10):1767+, 1998.

[15] T. Fulop and P. Helander. Nonlinear neoclassical transport in a rotating impure plasma with large gradients. *Doktorsavhandlingar vid Chalmers Tekniska Hogskola*, 3066(1538):3066–3075, 1999.

[16] C Angioni and P Helander. Neoclassical transport of heavy impurities with poloidally asymmetric density distribution in tokamaks. *Plasma Physics and Controlled Fusion*, 56(12):124001–124008, 2014.

[17] J. A. Wesson. Poloidal distribution of impurities in a rotating tokamak plasma. *Nuclear Fusion*, 37(5):577, 1997.

[18] T. Fülöp and P. Helander. Nonlinear neoclassical transport in toroidal edge plasmas. *Contributions to Plasma Physics*, 42(2-4):339–349, 2002.

[19] E A Belli, J Candy, and C Angioni. Pfirsch-Schluter neoclassical heavy impurity transport in a rotating plasma. *Plasma Physics and Controlled Fusion*, 56(12):124002, 2014.

[20] C. Angioni, F. J. Casson, P. Mantica, T. Pütterich, M. Valisa, E. A. Belli, R. Bilato, C. Giroud, and P. Helander. The impact of poloidal asymmetries on tungsten transport in the core of JET H-mode plasmas. *Physics of Plasmas*, 22(5), 2015.

[21] K.W. Wenzel and D.J. Sigmar. Neoclassical analysis of impurity transport following transition to improved particle confinement. *Nuclear Fusion*, 30(6):1117–1127, 2011.

[22] E A Belli and J Candy. An Eulerian method for the solution of the multi-species drift-kinetic equation. *Plasma Physics and Controlled Fusion*, 51(7):75018, 2009.

[23] P. H. Rutherford. Impurity transport in the Pfirsch-Schluter regime. *Physics of Fluids*, 17(9):1782, 1974.

[24] B Alper, R Giannella, K Lawson, F Marcus, M Mattioli, P Smeulders, and M Von Hellermann. Impurity Transport of High Performance Discharges in JET. pages 3–7.

[25] F. L. Hinton and S. K. Wong. Neoclassical ion transport in rotating axisymmetric plasmas. *Physics of Fluids*, 28(10):3082, 1985.

[26] W Choe, C S Chang, and M Ono. Temperature anisotropy in a cyclotron resonance heated tokamak plasma and the generation of poloidal electric field. *Physics of Plasmas*, 2:2044–2054, 1995.

[27] Ye O Kazakov, I Pusztai, T Fülöp, and T Johnson. Poloidal asymmetries due to ion cyclotron resonance heating. *Plasma Physics and Controlled Fusion*, 54(10):105010, 2012.

[28] C Angioni, M Sertoli, R Bilato, V Bobkov, A Loarte, R Ochoukov, T Odstrcil, T Pütterich, J Stober, The Asdex, and Upgrade Team. A comparison of the impact of central ECRH and central ICRH on the tungsten behaviour in ASDEX Upgrade H-mode plasmas. *Nucl. Fusion*, 57(056015), 2017.